Acta Scientiarum
http://periodicos.uem.br/ojs/acta
ISSN on-line: 1807-8664
Doi: 10.4025/actascitechnol.v47i1.69697

Deciphering Motor Imagery EEG Signals of Unilateral Upper Limb Movement using EEGNet

Kiruthika Krishnamoorthy* **and Ashok Kumar Loganathan**

Department of Electrical and Electronics Engineering, Thiagarajar College of Engineering, Madurai, 625015, Tamil Nadu, India. *Author for correspondence. E-mail: kiruthikakr596@gmail.com

ABSTRACT. Brain Computer Interfaces (BCI) face challenges in achieving sufficient control dimensions from decoding movements of left and right limb. To address this limitation, the motor imagery (MI) of fine movements from the same arm or leg can provide natural control of external equipment and increase the available control dimensions in a BCI system. However, conventional feature extraction and machine learning techniques have shown limited potential in detecting variations in EEG signals during the imagination of movements involving unilateral limb joints. In this study, we analyse the classification of movements specific to a single limb by utilizing EEGNet. We investigate the performance of EEGNet in classifying three different states: right-hand MI, right-elbow MI, and the rest state EEG signal. Our findings demonstrate that EEGNet achieves mean classification accuracy of 71.24% for the three-class classification task. The lowest accuracy observed was 58.89%, while the highest classification accuracy reached 84.44%. The results indicate that EEGNet has the potential to effectively differentiate MI signals of joints located on the same limb, offering promising avenues for intuitive control of external equipment in BCI applications. By surpassing the limitations of conventional techniques, EEGNet opens up new possibilities for improving control dimensions and enhancing the functionality of BCI systems.

Keywords: brain computer interface; electroencephalogram; intuitive control; stroke; convolutional neural networks; support vector machine.

Received on September 21, 2023.
Accepted on August 22, 2024.

Introduction

Traditional stroke rehabilitation methods involve physical exercise that a physiotherapist supervises. In contrast, active rehabilitation enables subjects to execute deliberate movements with their paralyzed extremities, thereby promoting neuroplasticity in the brain (Cassidy & Cramer, 2017). Utilizing Electroencephalogram (EEG) based BCI can enable individuals to operate a device or directly engage with the external space using their brain activations (Yadav & Maini, 2023). Compared to other BCI protocols, like those involving evoked and P300 potentials, MI-based BCI has the potential to be self-contained and indicative of the individual's intentional movement perception. Thus, MI-based BCI has a distinct advantage in stroke rehabilitation because it uses active imagery to stimulate the plastic potential of neurons to reconstruct control functions between the limb and brain (Hong et al., 2017).

The predominant area of research in MI- BCI pertains to the classification of movement intention into distinct categories, namely left or right arm, left or right leg, or a combination of arm, leg, and tongue movements (Padfield et al., 2022), because the cerebral site of event-related de-synchronization/synchronization is on separate regions of the brain when left- and right-limb MI is performed (Pfurtscheller & Lopes da Silva, 1999). There are two main limitations in using these multi-lateral task-based BCI systems: (i) The system exhibits low-dimensional control, implying a limited ability to distinguish a restricted set of cognitive tasks as specific control directives. (ii) The mental process of envisioning movements of distinct limbs to manipulate a peripheral device can lead to cognitive dissonance, characterized by a discrepancy between the intended movement goal and the actual action. For example, it is unnatural for the users to imagine moving both hands to propel the helicopter forward (Doud et al., 2011). Hence, only a few BCI are suited for real-world applications.

The MI paradigm involving multiple parts of the same limb can provide a natural means of controlling external equipment, such as an exoskeleton, without imposing additional cognitive stress on the user. This

approach avoids the need for the user to establish any artificial connections between imagined and neuroprosthetic movements. Using EEG signals to differentiate the MI of distinct actions within a limb is problematic since these MI have contiguous spatial depiction in the motor cortex (Sanes et al., 1995). Nonetheless, it is an urgent necessity to complete this task successfully. On the contrary, there are fewer investigations on multitasking MI-BCIs of the same extremity. Table 1 provides a survey on the available unilateral MI BCI tasks.

Table 1. MI studies focused on classifying intuitive movement tasks.

Reference	No of classes	MI tasks	Feature extraction	ML Algorithms	Accuracy
Vučković and Sepulveda (2012)	4	Extension, flexion, pronation, and supination	Gabor transform	ENN	63 ± 10%
Edelman et al. (2016)	4	Imaginary wrist movements	Time-frequency features	Extended EEG source imaging method	81.4%
Liao et al. (2014)	2	Ten pairs of finger movements	PCA and power spectral features	SVM	77.1%
Yong and Menon (2015); Tavakolan et al. (2017)	3	Rest, grasp, elbow, and elbow with goal	CSP, FBCSP and log band power, time-domain features, autoregressive model coefficients, waveform length, root mean square	LDA, SVM, LR Multiclass SVM	60.7%, 74.2%
Chu et al. (2020)	6	Wrist flexion, extension, pronation, and supination; hand close and open	CSP, FBCSP, Riemannian Geometry feature extraction	LDA and SVM classifier	80.50%
Alazrai, Alwanni, Baslan, Alnuman, and Daoud (2017)	11	Rest, three types of grasps, wrist ulnar/radial deviation, flexion and extension of five fingers separately	Choi-Williams time-frequency distribution	Binary and multiclass SVM	90.2%
Zhang et al. (2017)	2	Rest vs task (MI Tasks: elbow flexion /extension; opening /closing draw; drinking with a spoon; lifting and putting down a dumbbell; open/close a door; cleaning a plate; combing hair; cutting a pizza; and pick a ball and put it into basket	FBCSP	LDA and dual-augmented Lagrangian method	55% to 62%
Ma et al., (2020b)	3	Rest, right hand and right elbow	Sliding window approach, correlation matrix and coherence matrix	Channel-Correlation Network	87.03%
Zhou et al. (2009)	2	Torque at the shoulder or elbow	Time-frequency synthesized spatial patterns and transforms	SVM	92% in healthy and 75% in paretic
Ma et al. (2022)	5	Hand, wrist, elbow, shoulder, and rest	CSP and time distributed attention module	LSTM	46.8 % for 5 classes; 53.4 % for 4 classes
Lee et al. (2021)	4	Tappimg of index, middle, ring, and little finger	CSP	SVM, LDA, kNN, ESD and GNB	46.94 ± 5.99% for healthy; 66.0 ± 14.96% for stroke patients
Bi and Chu (2023)	6	Flexion and extension of elbow, pronation and supination of forearm, open and close hand	-	Transfer data learning network	65 ± 0.5%
Rao et al. (2024)	4	Thumb and finger flexion of the left and right hand	-	EEGNet with an attention module	72.91%
Satam (2024)	3	Rest, right hand, right elbow	Wavelet transform	ANFIS	90%
Guo et al. (2024)	2	Knee flexion and extension	Superlet transform	SVM	78.32%

Abbreviations used in Table: ANFIS- Adaptive Neuro Fuzzy Inference System, CSP- Common Spatial Pattern, ENN- Elman's Recurrent Neural Networks, ESD- Ensemble Subspace Discriminant, FBCSP- Filter-Bank CSP, GNB- Gaussian Naïve Bayes, kNN- k Nearest Neighbor, LDA- Linear Discriminant Analysis, LR- Logistic Regression, LSTM- Long-short Term Memory, PCA- Principal Component Analysis, SVM- Support Vector Machine

Several studies have concentrated on categorizing distinct MI tasks, including wrist movements, finger movements, hand grasping, and elbow movements as seen in Table 1. Diverse techniques for feature extraction are utilized, and various ML techniques are employed to decipher MI signals. The attained levels of accuracy exhibit variability in different studies, with values ranging from comparatively low (46%) to high

(92%). Few researchers have shown that ML algorithms can decode MI from paretic patients (Alazrai et al., 2017; Zhou et al., 2009; Lee et al., 2021). It is appropriate to evaluate the neural network's efficacy in classifying imagined joint motions of the same limb to enhance the probability of developing an intuitively operable robotic rehabilitation device. Due to its effectiveness and computational efficiency, EEGNet, a deep learning architecture for EEG data interpretation, has attracted much attention lately. Lawhern et al. (2018) first presented the EEGNet and the use of temporal and spatial convolutions in the EEGNet encapsulates the temporal and spatial features of the EEG without the need for any feature extraction approach. The performance of this EEG-specific convolutional neural network was assessed using multiple benchmark EEG datasets, which encompasses the evoked potential paradigm, the sensory-motor rhythm, and the movement-related cortical potential paradigm. The results show that it is more accurate, generalized, and efficient than conventional EEG analysis methods. EEGNet is effective in diagnosing various neurological conditions and for classifying diverse cognitive states such as concentration, drowsiness, and meditation (Peng et al., 2022). Recently architectural modifications have been proposed for the EEGNet architecture to improve its performance for single-trial EEG classification (Zhang et al., 2022). The present investigation employs EEGNet for categorizing unilateral right arm MI. This study uses openly available datasets from Harvard Dataverse (Ma et al., 2020a).

Material and methods

EEGNet is a deep learning architecture designed for EEG-based BCI and can capture local and global features. Its architecture, as shown in Figure 1, consists of several essential convolution layers, which makes it feasible to learn spatial and temporal features. Feature maps representing data flow across the layers in the neural network is shown in Figure 2. The first temporal convolutional layer operates on the temporal aspect of the EEG signals to learn frequency filters. The second layer of convolution learns frequency-specific spatial filters by employing two tasks: depthwise convolution and pointwise convolution. It learns to fuse the feature maps optimally and helps reduce the number of parameters and computations required by the network. Batch normalization employed after each convolution layer of EEGNet normalizes the activations between each layer, which helps prevent overfitting and stabilizes the network's training. Global average pooling averages the activations over all time points and helps reduce the count of parameters and computations. EEGNet also uses dropout to prevent overfitting and improve generalization. A dense layer is avoided for feature accumulation ahead of the final stage to limit the free parameters. In blocks 1 and 2, the model uses the elu activation, while in block 3 softmax activation is used.

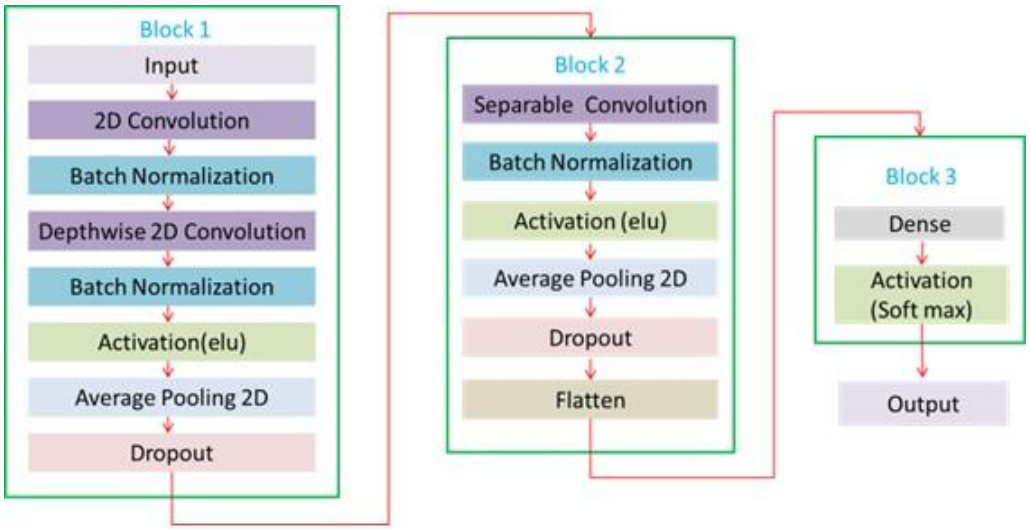

Figure 1. Schematic layout of blocks in EEGNet.

The open-access data from Harvard Dataverse was used. Twenty-five healthy participants completed three tasks in this study totaling 22,500 trials. The tasks include imagining the movement of (i) hand, (ii) elbow, and (iii) relaxing with eyes open. The EEG signals were recorded using a 64-channel Neuroscan SynAmps2 amplifier. The target cue ("Hand" or "Elbow") was displayed for four seconds as a visual cue and the order of task cues in a session was randomized. The participants were instructed to kinesthetically imagine the

indicated movement. The experiment consists of 300 trials of resting state collected over four sessions (4x75 trials) and 15 sessions of 40 trials of hand and elbow MI (20 trials for hand and 20 trials for elbow in a session). Thus, the dataset contains 300 trials for each type of mental state for each individual. The data were collected at 1 kHz sampling rate and subjected to 0.5–100 Hz band-pass filtering followed by a 50 Hz notch filter. The data were spatially filtered using common average reference and time-domain filtering from 0 to 40 Hz. In order to cut down on processing costs, the data were down-sampled to 200 Hz. The muscle and eye movement artifacts were eliminated using the automatic artifact removal toolkit.

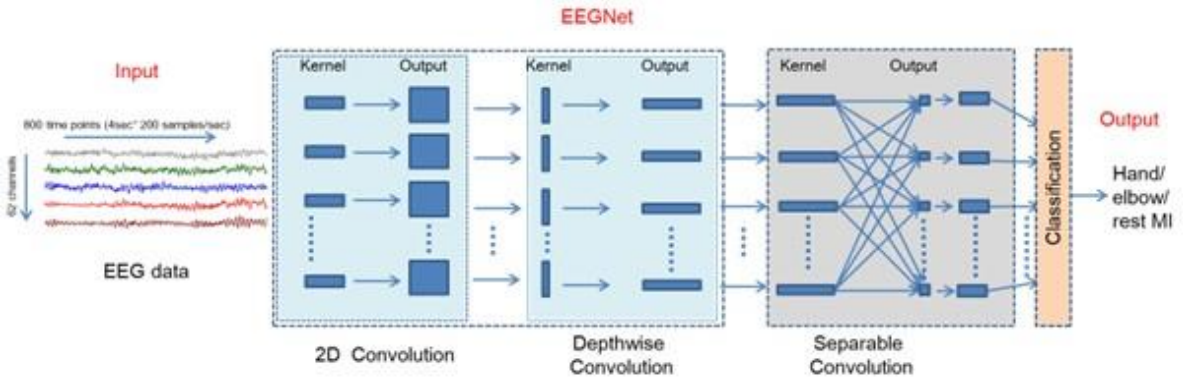

Figure 2. Visualization of the information extraction by the 2D convolution layers in the EEGNet.

The procedure adopted for classifying the EEG signal is illustrated in the block diagram, as shown in Figure 3. First, the data set in '.mat' format is downloaded from the Harvard Dataverse. The 25 patients' EEG data from .mat files are classified using a subject-dependent or within-subject technique. The .mat files of each patient contain 600 trials of task data, 600 task labels, and 300 trials of rest data. These data are read into the Python workspace into data and label variables. The data is validated for the presence of any missing and infinity values. In step two, the EEGNet model is defined and compiled with sparse categorical cross entropy loss function and with required early stopping parameters. The EEGNet model is modified to suit the dataset by setting the kernel length to 100, which is half the sampling frequency of the data. In step 3, the model is trained in the subject-wise method using a validation technique.

The 900 trials of 62-channel EEG data of a subject are randomized and divided into a train, validation, and test set. The training set included 720 samples (80%), and validation and testing were done using the remaining 20% of data each (90 samples for testing and 90 samples for validation). At the end of each epoch, 90 samples are used to validate the model. Finally, the learned model at the end of training is tested using the test data, and its accuracy in classifying unseen data is analyzed.

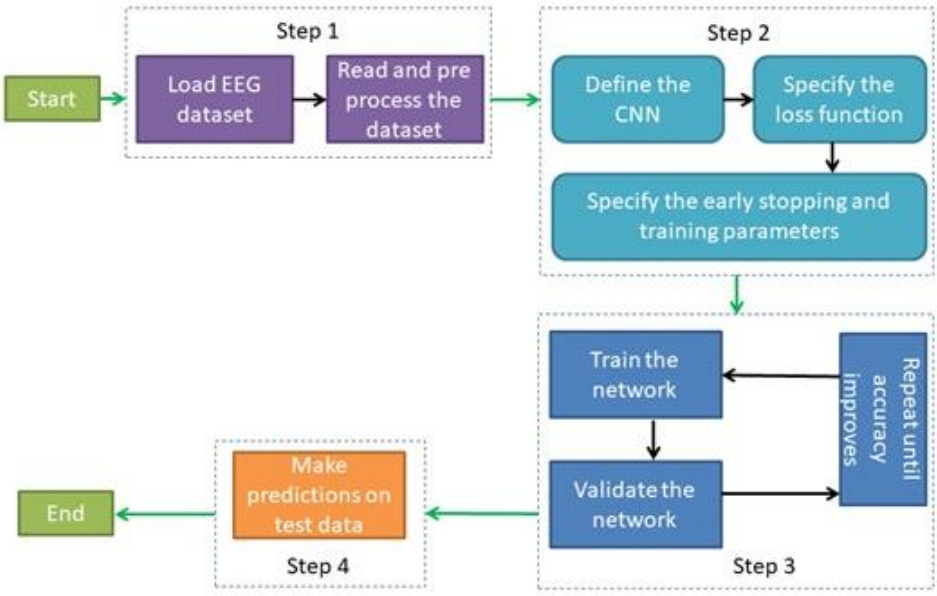

Figure 3. Block Diagram of the methodology.

The Google Collab notebook is used to train and test the EEGNet. The model is trained with an upper limit of 500 epochs, but early stopping with a patience value of 50 reduces processing time and avoids overfitting. Sparse categorical cross entropy is the loss function used. The best weights are restored at the end of each training fold, and the validation loss is monitored for early stopping. During model training, network weights are iteratively updated using the Adam optimizer.

The input of shape (none, 62, 800,1) is fed to the input layer of the EEGNet. The EEG data is passed to the first 2D convolution layer where eight filters of size (1, 100) are convolved with the data to produce eight feature maps containing EEG signals at different frequency bands, which produces an output of shape (none, 62, 800,8). Next, a depth-wise convolution filter of size (62, 1) and a depth of 2 are used to obtain the spatial filter, which provides an output of shape (none, 1, 800, 16). Both convolutions in block one are performed linearly, and batch normalization is performed after each convolution step. Drop out of 0.5 is used to regularize the model and prevent overfitting. In block 2, a depth-wise convolution of size (1,16) succeeded by 32 point-wise convolutions of size (1,1) is done to limit the parameters to fit. An average pooling layer of size (1, 8) is employed for dimension reduction. After the dropout, the output shape of block two is (None, 1, 25, 16). Now the classification layer only has these few data to classify the output into the three classes. The final dense layer connects all the 400 flattened layers to the final softmax activation layer.

Results and discussion

Table 2 shows the classification accuracy for all 25 subjects while considering all 62 channels of data. The three-class classification accuracy of the FBCSP feature extraction and SVM classifier reported by Ma et al. (2020a) for the same dataset is also shown in Table 2 and Figure 4. The proposed EEGNet showed an average accuracy of 71.24% for the ternary classification. The best classification accuracy of EEGNet was found to be 84.44% for subjects 7 and 16. The lowest classification accuracy of 58.89% was obtained for subjects 11 and 20. Inter-subject variability in EEG signals can make it challenging to develop a model that works well for all subjects.

Table 2. Classification performance of FBCSP+SVM and EEGNet.

Subjects	FBCSP+SVM Accuracy	EEGNet			
		Accuracy	AUC		
			Rest	Hand	Elbow
S001	69	71.11	0.98	0.84	0.80
S002	68.11	74.44	0.97	0.79	0.86
S003	71.67	71.11	0.96	0.84	0.81
S004	69	73.33	0.98	0.79	0.85
S005	66.33	71.11	0.96	0.84	0.81
S006	73.44	70.00	0.96	0.85	0.82
S007	63.78	84.44	0.97	0.93	0.92
S008	67.33	63.33	0.92	0.73	0.73
S009	71.89	78.89	0.97	0.92	0.93
S010	70.78	72.22	0.97	0.79	0.86
S011	68.89	58.89	0.90	0.67	0.71
S012	71.67	67.78	0.96	0.73	0.76
S013	67.67	66.67	0.95	0.77	0.75
S014	67.44	72.22	0.92	0.83	0.84
S015	71.33	76.67	0.95	0.82	0.80
S016	69.11	84.44	0.98	0.93	0.93
S017	67.78	77.78	0.98	0.91	0.88
S018	67.11	77.78	0.97	0.89	0.86
S019	62.44	63.33	0.94	0.76	0.75
S020	67.78	58.89	0.87	0.74	0.68
S021	69.89	60.00	0.92	0.71	0.68
S022	66.78	76.67	0.96	0.84	0.84
S023	70.22	75.55	0.95	0.82	0.85
S024	68	65.55	0.94	0.86	0.82
S025	68.68	68.89	0.95	0.78	0.82
Average	68.64	71.24	0.95	0.82	0.81

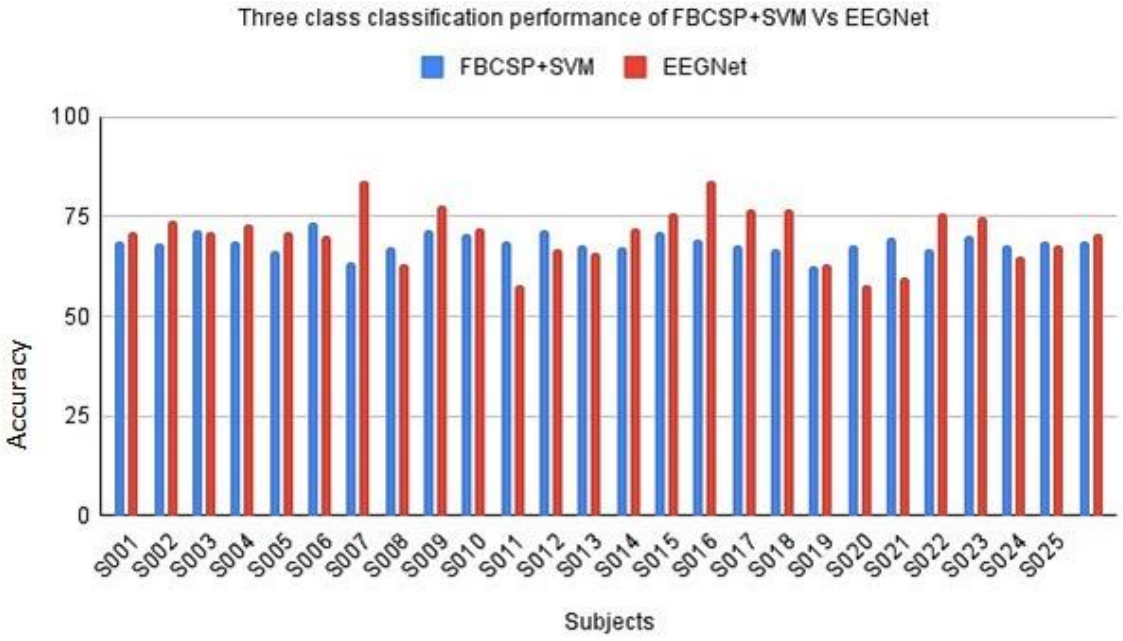

Figure 4. Three class classification performance of EEGNet and FBCSP+SVM.

With an average accuracy of approximately 71.24% for classifying rest, hand movement MI, and elbow movement MI, it is evident that EEGNet effectively discerns MI of the same limb joints using the local and global information gathered by its spatial and temporal filters. For Subject 1, with an accuracy of 71.11%, the confusion matrix and Receiver Operating Characteristics (ROC) curve are depicted in Figure 5. The confusion matrix summarizes the EEGNet performance on the test data and the One-vs-Rest (OvR) ROC curve illustrates the separability of a class against the other classes across all possible threshold values.

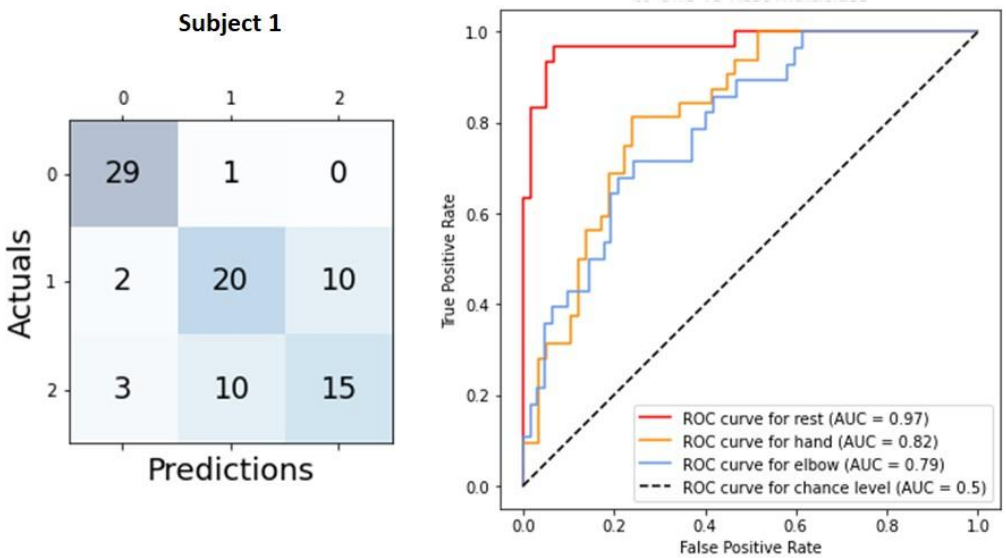

Figure 5. Confusion matrix (left) and OvR ROC curve(right) for Subject 1 (Labels in Confusion matrix: 0-rest; 1-hand MI; 2-elbow MI).

In Figure 6, the confusion matrix and ROC curve for the highest classification accuracy of 84.44% are shown. The Area Under the ROC curve (AUC) values for all three classes are above 0.92, demonstrating that EEGNet can easily decipher the three classes of MI in subjects 7 and 16. Figure 7 presents the confusion matrix and ROC curve for the lowest classification accuracy of 58.89%. Here, the AUC value for distinguishing rest state from the other two MI classes exceeds 0.85, indicating that EEGNet can better classify rest state against hand and elbow MI. The AUC values for hand MI versus the other classes and elbow MI versus the other classes are 0.67 and 0.71 for Subject 11 and 0.70 and 0.67 for Subject 20. These values are significantly above the chance level of 0.5, suggesting that the model can reliably differentiate these classes at all possible threshold values.

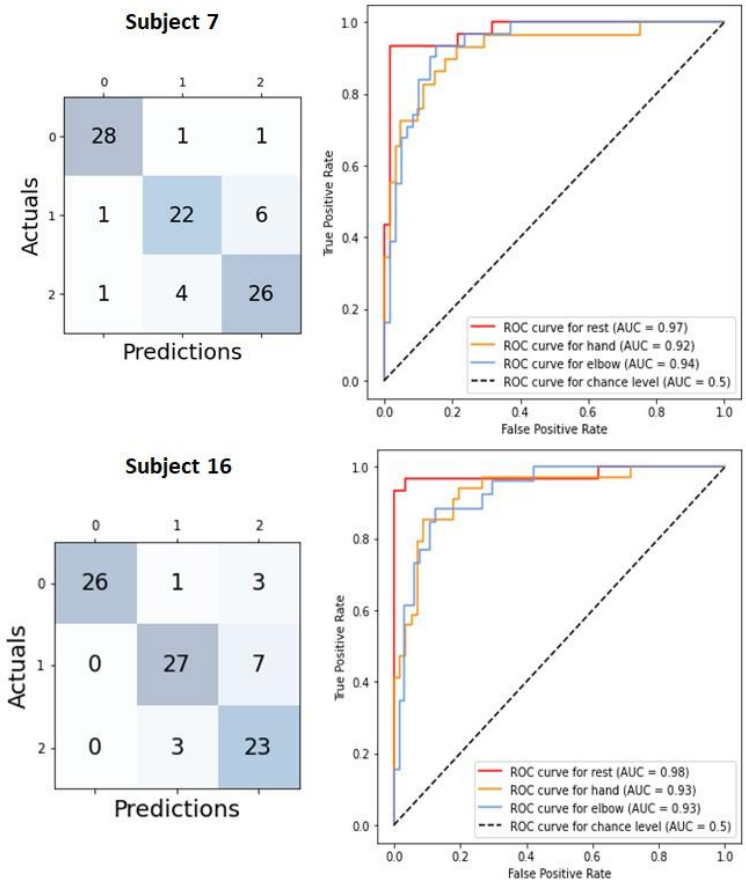

Figure 6. Confusion matrix (left) and OvR ROC curve (right) for highest classification accuracy (Labels in Confusion matrix: 0-rest; 1-hand MI; 2-elbow MI).

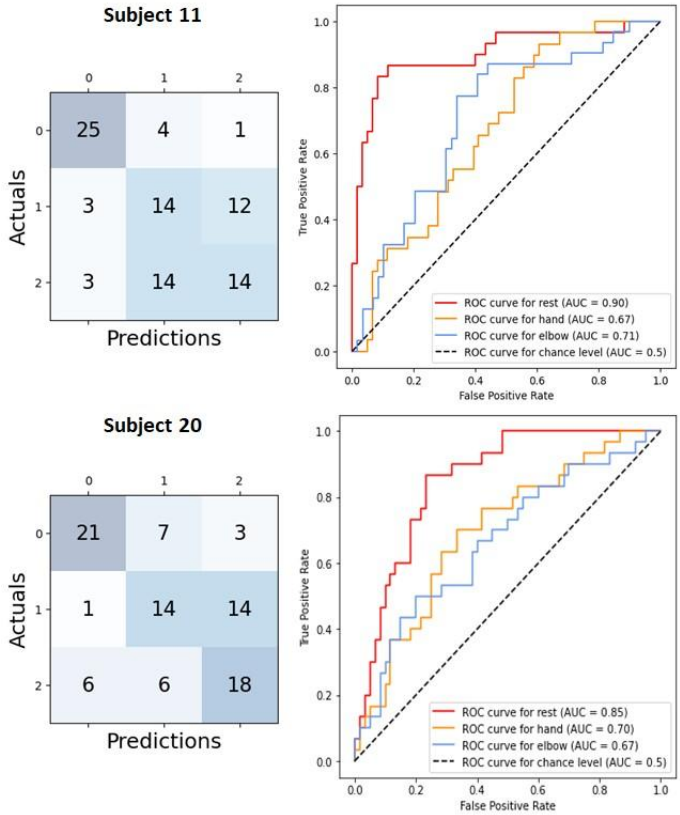

Figure 7. Confusion matrix (left) and OvR ROC curve (right) for lowest classification accuracy (Labels in Confusion matrix: 0-rest; 1-hand MI; 2-elbow MI).

The model can better classify the {rest} against {hand and elbow}, while {elbow} vs {rest, hand} and {hand} vs {elbow, rest} have an AUC on the same level as observed in Table 2. The highest classification accuracy of FBCSP+SVM and EEGNet is 71.89 and 84.88% respectively. An improvement in classification accuracy is achieved in three-class classification using EEGNet. Automatic feature learning of EEGNet has learned relevant features directly from raw EEG data. This eradicates the subjective manual feature engineering step and can capture complex patterns in the EEG signals without relying on pre-defined features. EEGNet also enables end-to-end learning, where it learns directly from the raw EEG data to the desired classification labels. This holistic approach allows the model to optimize all the parameters simultaneously, resulting in better performance than traditional methods involving separate feature extraction and classification steps.

Data availability

Open access data from Harvard dataverse is used in this study. The link to the data source is https://doi.org/10.7910/DVN/RBN3XG

Conclusion

The average classification accuracy for the ternary problem of deciphering rest from imaginary hand and elbow MI is 71.24%, more significant than the random classification accuracy of 33%. In addition, the EEGNet-based classification outperformed the FBCSP+SVM with an overall success rate of 71.24% versus 68.64%. The findings show that it is possible to interpret the same limb movements with EEGNet to give a natural way to manage the external devices and offer the opportunity to enhance the possible degrees of freedom of equipment controlled by a BCI. This could open the door to other exoskeletons and robotic devices that the user can operate directly rather than depending on external commands or unrelated movement ideas.

References

Alazrai, R., Alwanni, H., Baslan, Y., Alnuman, N., & Daoud, M. (2017). EEG-Based Brain-Computer Interface for Decoding Motor Imagery Tasks within the Same Hand Using Choi-Williams Time-Frequency Distribution. *Sensors*, *17*(9), 1937. https://doi.org/10.3390/s17091937

Bi, J., & Chu, M. (2023). TDLNet: Transfer Data Learning Network for Cross-Subject Classification Based on Multiclass Upper Limb Motor Imagery EEG. *IEEE Transactions on Neural Systems and Rehabilitation Engineering*, *31*, 3958-3967. https://doi.org/10.1109/tnsre.2023.3323509

Cassidy, J. M., & Cramer, S. C. (2017). Spontaneous and Therapeutic-Induced Mechanisms of Functional Recovery after Stroke. *Translational stroke research*, *8*(1), 33-46. https://doi.org/10.1007/s12975-016-0467-5

Chu, Y., Zhao, X., Zou, Y., Xu, W., Song, G., Han, J., & Zhao, Y. (2020). Decoding multiclass motor imagery EEG from the same upper limb by combining Riemannian geometry features and partial least squares regression. *Journal of Neural Engineering*, *17*(4), 046029. https://doi.org/10.1088/1741-2552/aba7cd

Doud, A. J., Lucas, J. P., Pisansky, M. T., & He, B. (2011). Continuous Three-Dimensional Control of a Virtual Helicopter Using a Motor Imagery Based Brain-Computer Interface. *PLoS ONE*, *6*(10), e26322. https://doi.org/10.1371/journal.pone.0026322

Edelman, B. J., Baxter, B., & He, B. (2016). EEG Source Imaging Enhances the Decoding of Complex Right-Hand Motor Imagery Tasks. *IEEE Transactions on Biomedical Engineering*, *63*(1), 4-14. https://doi.org/10.1109/tbme.2015.2467312

Guo, Y., Wan, L., Sheng, X., Wang, G., Kang, S., Zhou, H., & Zhang, X. (2024). The Application of Superlet Transform in EEG-Based Motor Imagery Classification of Unilateral Knee Movement. In *Lecture notes in electrical engineering,* 511-521. https://doi.org/10.1007/978-981-97-1087-4_48

Hong, X., Lu, Z. K., Teh, I., Nasrallah, F. A., Teo, W. P., Ang, K. K., Phua, K. S., Guan, C., Chew, E., & Chuang, K. H. (2017). Brain plasticity following MI-BCI training combined with tDCS in a randomized trial in chronic subcortical stroke subjects: a preliminary study. *Scientific Reports*, *7*(1). https://doi.org/10.1038/s41598-017-08928-5

Lawhern, V. J., Solon, A. J., Waytowich, N. R., Gordon, S. M., Hung, C. P., & Lance, B. J. (2018). EEGNet: a compact convolutional neural network for EEG-based brain–computer interfaces. *Journal of Neural Engineering*, *15*(5), 056013. https://doi.org/10.1088/1741-2552/aace8c

Lee, M., Jeong, J. H., Kim, Y. H., & Lee, S. W. (2021). Decoding Finger Tapping With the Affected Hand in Chronic Stroke Patients During Motor Imagery and Execution. IEEE *transactions on neural systems and rehabilitation engineering: a publication of the IEEE Engineering in Medicine and Biology Society*, *29*, 1099-1109. https://doi.org/10.1109/tnsre.2021.3087506

Liao, K., Xiao, R., Gonzalez, J., & Ding, L. (2014). Decoding Individual Finger Movements from One Hand Using Human EEG Signals. *PLoS ONE*, *9*(1), e85192. https://doi.org/10.1371/journal.pone.0085192

Ma, X., Qiu, S., & He, H. (2020a). Multi-channel EEG recording during motor imagery of different joints from the same limb. *Harvard Dataverse*. https://doi.org/10.7910/DVN/RBN3XG

Ma, X., Qiu, S., Wei, W., Wang, S., & He, H. (2020b). Deep Channel-Correlation Network for Motor Imagery Decoding from the Same Limb. *IEEE Transactions on Neural Systems and Rehabilitation Engineering*, *28*(1), 297-306. https://doi.org/10.1109/tnsre.2019.2953121

Ma, X., Qiu, S., & He, H. (2022). Time-Distributed Attention Network for EEG-Based Motor Imagery Decoding From the Same Limb. *IEEE Transactions on Neural Systems and Rehabilitation Engineering*, *30*, 496-508. https://doi.org/10.1109/tnsre.2022.3154369

Padfield, N., Camilleri, K., Camilleri, T., Fabri, S., & Bugeja, M. (2022). A Comprehensive Review of Endogenous EEG-Based BCIs for Dynamic Device Control. *Sensors*, *22*(15), 5802. https://doi.org/10.3390/s22155802

Peng, R., Zhao, C., Jiang, J., Kuang, G., Cui, Y., Xu, Y., Du, H., Shao, J., & Wu, D. (2022). TIE-EEGNet: Temporal Information Enhanced EEGNet for Seizure Subtype Classification. In *IEEE Transactions on Neural Systems and Rehabilitation Engineering* (pp. 2567-2576). https://doi.org/10.1109/tnsre.2022.3204540

Pfurtscheller, G., & Lopes da Silva, F. H. (1999). Event-related EEG/MEG synchronization and desynchronization: basic principles. *Clinical neurophysiology: official journal of the International Federation of Clinical Neurophysiology*, *110*(11), 1842-1857. https://doi.org/10.1016/s1388-2457(99)00141-8

Rao, Y., Zhang, L., Jing, R., Huo, J., Yan, K., He, J., Hou, X., Mu, J., Geng, W., Cui, H., Hao, Z., Zan, X., Ma, J., & Chou, X. (2024). An optimized EEGNet decoder for decoding motor image of four class fingers flexion. *Brain Research*, *1841*, 149085. https://doi.org/10.1016/j.brainres.2024.149085

Sanes, J. N., Donoghue, J. P., Thangaraj, V., Edelman, R. R., & Warach, S. (1995). Shared Neural Substrates Controlling Hand Movements in Human Motor Cortex. *Science*, *268*(5218), 1775-1777. https://doi.org/10.1126/science.7792606

Satam, I. (2024). EEG signal ANFIS classification for motor imagery for different joints of the same limb. *Vojnotehnicki Glasnik*, *72*(1), 330-350. https://doi.org/10.5937/vojtehg72-46601

Tavakolan, M., Frehlick, Z., Yong, X., & Menon, C. (2017). Classifying three imaginary states of the same upper extremity using time-domain features. *PLoS ONE*, *12*(3), e0174161. https://doi.org/10.1371/journal.pone.0174161

Vučković, A., & Sepulveda, F. (2012). A two-stage four-class BCI based on imaginary movements of the left and the right wrist. *Medical Engineering and Physics*, *34*(7), 964-971. https://doi.org/10.1016/j.medengphy.2011.11.001

Yadav, H., & Maini, S. (2023). Electroencephalogram based brain-computer interface: Applications, challenges, and opportunities. *Multimedia Tools and Applications*, *82*, 47003–47047. https://doi.org/10.1007/s11042-023-15653-x

Yong, X., & Menon, C. (2015). EEG Classification of Different Imaginary Movements within the Same Limb. *PLoS ONE*, *10*(4), e0121896. https://doi.org/10.1371/journal.pone.0121896

Zhang, X., Yong, X., & Menon, C. (2017). Evaluating the versatility of EEG models generated from motor imagery tasks: An exploratory investigation on upper-limb elbow-centered motor imagery tasks. *PLoS ONE*, *12*(11), e0188293. https://doi.org/10.1371/journal.pone.0188293

Zhang, H., Wang, Z., Yu, Y., Yin, H., Chen, C., & Wang, H. (2022). An improved EEGNet for single-trial EEG classification in rapid serial visual presentation task. *Brain Science Advances*, *8*(2), 111-126. https://doi.org/10.26599/bsa.2022.9050007

Zhou, J., Yao, J., Deng, J., & Dewald, J. P. (2009). EEG-based classification for elbow versus shoulder torque intentions involving stroke subjects. *Computers in Biology and Medicine*, *39*(5), 443–452. https://doi.org/10.1016/j.compbiomed.2009.02.004